Gene 547 (2014) 319–328

Contents lists available at ScienceDirect

Gene

journal homepage: www.elsevier.com/locate/gene

Identification of a microRNA regulator for axon guidance in the olfactory bulb of adult mice

Tingting Sun [a], Shanshan Li [a], Jing Yang [a], Yifei Yin [b], Shucai Ling [a,*]

[a] Institute of Neuroscience and Anatomy, Zhejiang University School of Medicine, Hangzhou, China
[b] Institute of Life Science, Zhejiang University, Hangzhou, China

ARTICLE INFO

Article history:
Received 11 March 2014
Received in revised form 25 June 2014
Accepted 27 June 2014
Available online 30 June 2014

Keywords:
Axon guidance
Semaphorin3A
Olfactory bulb
miR-30c

ABSTRACT

Semaphorin3A (sema3a), mainly localized in the olfactory neuron layer and periglomerular layer, is essential for the normal arrangement of axons in the olfactory bulb both in embryonic and adult mice functioning through its dynamic spatiotemporal expression. The regulators that can modulate the expression of sema3a by direct interaction, however, are unknown. In order to find the regulators of sema3a in the olfactory bulb, we focused on microRNAs, well-known post-transcriptional regulators. We found that axon guidance is the main molecular and biological process ongoing in the steady-state olfactory bulb of the adult mouse by screening the abundant microRNAs and exploring their functions in the olfactory bulb *via* our customized microRNA arrays, Gene Ontology and Kyoto Encyclopedia of Genes annotation. Furthermore, we traced the expression of three candidate regulators (miR-30c, miR-200b, and miR-429) and sema3a by the quantitative real-time polymerase chain reaction and immunohistochemistry. The results showed that only miR-30c expression corresponded inversely with sema3a. Finally, miR-30c was verified to be a specific regulator of sema3a by dual luciferase reporter assay *in vitro*. Taken together, our results suggested that miR-30c is a potential regulator in axon-guidance by suppressing the expression of sema3a, which will give new insights in elucidating the mechanism of architectonic and functional maintenance of the olfactory bulb.

1. Introduction

Axon guidance plays a key role in establishing neuronal circuitry and it is the process by which neurons send out axons to reach their correct targets, navigating by molecular cues. It has been established that the direction of axon protrusion is defined by the guidance cues acting on the growth cone, a highly motile structure at the growing tip. Growth cones 'sense' guidance cues *via* receptors and then the signal is transduced into chemotropic responses (Tessier-Lavigne and Goodman, 1996). So far, many classes of axon-guidance molecules and their receptors such as netrins (DCC and UNC5), slits (Robo), ephrins (Eph), semaphorins (plexins and neuropilins) have been found to play as repellent or attractive cues for axon guidance in different nervous systems (Causeret, 2006; Cohen et al., 2003; Finger et al., 2002; Lakhina et al., 2012; Puschmann and Turnley, 2010; Sweeney et al., 2011).

Semaphorins are a class of membrane-associated secreted and transmembrane proteins that contain the highly-conserved semaphorin domain; they have been implicated in axon guidance from flies to vertebrates (Chen et al., 1998). Semaphorin3A (Sema3a) was initially found based on its ability to induce the collapse of growth cones of dorsal root ganglion cells, and it is required to form the projection pattern in the peripheral nervous system (Luo et al., 1993; Taniguchi et al., 1997). Sema3a is also essential in olfactory axon projection during embryonic development; sema3a-deficient mice have abnormal neurophilin-1-positive axon projections in the olfactory bulb (OB) (Schwarting et al., 2000). Moreover, sema3a is engaged in the maintenance of circuit' patterns in adult OB; sema3a-deficient mice have a distorted odor map in which the neurophilin-1-positive glomeruli are ectopically arranged in the anteromedial and ventral regions (Taniguchi et al., 2003). Recently, sema3a has been confirmed to regulate neuronal polarization by suppressing axon formation and promoting dendrite growth. During this process, sema3a activates a specific signal pathway that switched on dendritic growth-related molecules and switches off axon extension-related molecules *via* the pivotal molecules cAMP and cGMP (Shelly et al., 2011).

It has been reported that it is the relative expression of guidance molecules, rather than their absolute expression levels, that enables them to function as axon-guidance cues. In developing cortical layers, Sema3a shows a descending gradient with highest expression at the

Abbreviations: Quantitative RT-PCR, quantitative real-time polymerase chain reaction; LNA, locked nucleic acid; GO, gene ontology; GO BP, gene ontology biological process; GO CC, gene ontology cellular component; GO MF, gene ontology molecular function; KEGG, Kyoto Encyclopedia of Genes and Genomes; OB, olfactory bulb; Sema3a, semaphorin3A; OSN, olfactory sensory neuron; FDR, false discovery ratio.

* Corresponding author at: Institute of Neuroscience and Anatomy, Zhejiang University School of Medicine, 866 Yuhangtang Road, Hangzhou 310058, China.
E-mail address: lingshucai@zju.edu.cn (S. Ling).

http://dx.doi.org/10.1016/j.gene.2014.06.063
0378-1119/

pial surface; by this gradient, the axons of developing cortical neurons are oriented away from the pial surface (Polleux et al., 2000). *In vitro* experiments have shown that the dendrites of cultured hippocampal neurons preferentially orient towards a sema3a stripe while the axons orient away from the stripe. So the sema3a gradient acts as an axon-dendrite polarizing factor (Shelly et al., 2011). However, the factors that cause the expression gradient of sema3a are still unknown. Imai et al. reported that the expression of sema3a is reduced at high cAMP level (Imai et al., 2009). But the mechanism by which cAMP regulates the expression of sema3a remains elusive.

Recently, microRNAs have been found to play important roles in neuronal growth, differentiation and survival in the nervous systems (Cheng et al., 2009; Choi et al., 2008; de Chevigny et al., 2012). Baudet et al. (2013) suggested the potential of microRNAs to engage in regulation of axon guidance (Baudet et al., 2013). Besides, Martin et al. reported that both growing and mature axons possess a complex and dynamic transcriptome and this local mRNA translation can mediate directional responses to guidance signals (Martin, 2004), so microRNAs, well-known post-transcriptional regulators, probably regulate axon guidance by repressing their corresponding target mRNA in the local transcriptome of axons. To explore the roles of microRNAs in axon guidance, we first screened the abundant microRNAs and predicted their roles in the adult OB based on microRNA expression profile and bioinformatics methods respectively. Then, by a series of experimental verification, miR-30c was found to be a regulator of sema3a.

2. Materials and methods

2.1. Animals

Animal experimentation and use were approved by the Zhejiang University Animal Care and Use Committee and conformed to the international guidelines on the ethical use of animals. All efforts were made to minimize the number of animals used. Experimental animals were commercially-available male C57BL/6 mice (SLAC, Shanghai, China).

2.2. RNA isolation and microarray analysis

First, 8 week-old mice were deeply anesthetized with pentobarbital sodium and then the OBs were rapidly dissected from the fresh brains. Total RNA was harvested using TRIzol (Invitrogen, Carlsbad, CA, USA) and miRNeasy Mini Kit (Qiagen, Hilden, Germany) according to the manufacturer's instructions (n = 5 mice). The yield of total RNA was assessed using NanoDrop ND-1000 spectrophotometer (NanoDrop Technologies Inc., Rockland, DE) and the integrity of total RNA was determined by gel electrophoresis, then the samples were labeled using the miRCURY Hy3/Hy5 Power labeling kit and hybridized on the miRCURY LNA (locked nucleic acid, LNA) Array (version 16.0) (Exiqon, Vedbaek, Denmark) that contains more than 1891 capture probes in total, covering all human, mouse and rat microRNAs annotated in miRbase 16.0 (the total capture probes for mouse microRNAs are 1084; n = 3 mice). After washing, the slides were scanned using the Axon GenePix 4000B microarray scanner. Scanned images were then imported into GenePix Pro 6.0 software (Axon Instruments, Foster City, CA, USA) for grid alignment and data extraction. Four replicated values were averaged and those with intensities ≥50 in all samples were chosen to calculate the normalization factor. Expressed data were normalized using median normalization. Then, microRNA expression values that were ≥5 folds of the normalized median value of the whole array were selected. Finally, hierarchical clustering was performed to show the relative expression of miRNA profiles among samples (MeV software version 4.6, TIGR).

2.3. Quantitative RT-PCR analysis

The relative expression of miR-30a, miR-30b, miR-30c, miR-30d, miR-30e, miR-200b, miR-429, and miR-9 was determined by two-steps of qRT-PCR (expressions of miR-30a, miR-30b, miR-30d and miR-30e were traced at three time points: 4, 8 and 14 weeks; expressions of miR-30c, miR-9, miR-200b, miR-429 were traced at four time points: 4, 8, 14 and 19 weeks; n = 3–5 mice per time point). First, the cDNA of the microRNA was synthesized by RTase M-MLV (TakaRa, Dalian, China) using a stem-loop primer based on a previous described report (Chen et al., 2005; Wang et al., 2012). Then qRT-PCR reactions containing SYBR Green Mix (Invitrogen Carlsbad, CA, USA) were performed according to the manufacturer's instructions for CFX96 (Bio-Rad, CA, USA). The relative expression levels of sema3a were determined by quantitative two-step RT-PCR assays with gene-specific primer sets (Invitrogen, Shanghai, China) as previously described (Hojati and Orangi, 2012). The relative microRNA and mRNA levels were computed using the $2^{-\Delta\Delta Ct}$ method, where Snord2 (from our data, Snord2 was the best microRNA control, as it was constant with age comparing with the other two microRNA controls: 5sRNA and snordRNA234) and β-actin were used as internal controls for microRNA and mRNA respectively, and all reactions were run in triplicate.

2.4. Target prediction

The microRNA target prediction was based on three algorithms: TargetScan, Pita, and miRanda. TargetScan predication is based on searching for conserved 8-mer or 7-mer sites in mRNAs that match the seed regions of microRNAs, and the results can be ranked based on the predicted efficacy of targeting as calculated using the context + scores of the sites. Pita prediction is based on systematically investigating the role of target-site accessibility, which is determined by base-pairing interactions between microRNA and mRNA. miRanda prediction is also based on the matching of sites between the seed regions of microRNAs and mRNAs, but it divides the microRNA sequences into several regions, and evaluates the contribution of different regions of microRNA to the binding of mRNA. First, all executable file packages of these algorithms were downloaded and minor modifications were made based on our requirements. Then the prediction results from each algorithm underwent preliminary filtering based on their advantages. Finally, the intersections of screening results after preliminary filtering were used as the prediction results for the target genes of the 23 most abundant microRNAs.

2.5. Annotation and enrichment information

The annotation and enrichment of target genes were performed by DAVID (The Database for Annotation, Visualization and Integrated Discovery) (http://david.abcc.ncifcrf.gov/), which integrates the databases of the GO (Gene Ontology) and KEGG (Kyoto Encyclopedia of Genes) pathways together. The functional annotation and pathway analysis were performed using Fisher's exact test and the χ^2 test, where both the Expression Analysis Systematic Explorer (EASE) and False Discovery Ratio (FDR) were calculated to correct the p value as previously described (Han et al., 2012; Hosack et al., 2003). Enrichment provides a measure of the significance of terms in the annotation of GO and KEGG. Within the significant category, the enrichment was given by: enrichment = $(n_i / n) / (N_i / N)$ where n_i is the number of predicted target genes within a particular category, n is the total number of genes within the same category, N_i is the number of genes among the entire differential microRNA-corresponding target genes, and N is the total number of differential target genes in the microarray.

2.6. MicroRNA–mRNA network analysis

Cytoscape software and Network Analyzer plug-ins (version 1.0 http://med.bioinf.mpi-inf.mpg.de/netanalyzer/) were used to calculate

the basic network parameters: degree distribution, degree exponent, shortest path length distribution, and betweenness centrality. The scale of icons in the network represented the degree of contribution to the network. The greater contribution a node makes, the larger scale the icon has (Doncheva et al., 2012). The key microRNAs and genes in the network always have greater degrees. Pathway analyses were carried out using the ClueGO plug-in (version 1.4) in Cytoscape. Only pathways with both EASE < 0.01 and FDR < 0.01 were considered positive.

2.7. Immunohistochemistry

Adult mice with 4, 8, 14, and 19 weeks of age (n = 3–5 mice per age group) were deeply anesthetized with pentobarbital sodium and perfused with 0.1 M phosphate buffer (PB), pH 7.4, followed by 4% paraformaldehyde in PB. Brains were postfixed in 4% paraformaldehyde for 12 h and then kept overnight in cold PBS containing 30% sucrose. Coronal sections (20 μm) through the olfactory bulb were cut on a cryotome. The sections were first exposed to 0.3% H_2O_2 (final concentration in PBS) to reduce the endogenous peroxidase, then blocked with PBS containing 10% donkey serum (Santa Cruz, Los Angeles, CA, USA), and incubated with primary antibodies overnight at 4 °C. The primary antibodies used affinity-purified goat polyclonal antibodies raised against a peptide mapping near the C-terminal of sema3a (Santa Cruz, Q-18, 1/500 dilution). To ensure optimal results, we used the primary matched ABC staining system with biotinylated secondary antibody, avidin, and biotinylated horseradish peroxidase (sc-2023, Santa Cruz, Los Angeles, CA, USA). The negative control group was carried out with the same steps as described above, only the primary antibody was replaced by PBS.

For quantification, coronal sections that were about 0.48 mm posterior of the tip of olfactory bulb from different age groups were selected for comparison and the intensity of granule-cell layer in the lateral ventral was detected. To obtain the accurate data, the same gain and exposure settings were used for the digital capture of immunostaining images for each experiment. The intensity of sema3a was defined by the average optical intensity in a restricted area, that is, the value of integrated optical intensity divided by the restricted area (coronal sections of 4, 8, 14 and 19 weeks were detected; n = 3 mice per group). The intensity was calculated using Image-Pro Plus (IPP version 6.0).

2.8. Dual luciferase reporter assay

The construct sema3a-WT-3′UTR was obtained by annealing 58 bp of the 3′ UTR of sema3a (GI: 340523098, NM_009152) 5′-TCGAGATACACA TGAACATTTCATGGCATTATGTGGATGTTTACAATGATGGGAAGC-3′, containing a perfect putative miR-30c seed region binding site (underlined), to its complementary sequence. Sema3a-MUT-3′UTR was obtained by annealing the mutant 3′ UTR of sema3a 5′-TCGAGATACACATGAACATT TCATGGCATTATGTGGAT*CAAACT*AATGATGGGAAGC-3′, whose putative miR-30c seed region binding site (underlined) was mutated (italics), to its complementary sequence. Then the double sequences were ligated into the multiple cloning sites of the *Renilla*:firefly luciferase-expression vector psiCHECK-2 (Promega, Madison, USA). The sequences of psiCHECK-2-sema3a-WT-3′UTR and psiCHECK-2-sema3a-MUT-3′UTR thus obtained were validated by further sequencing.

The miR-30c expression vector was obtained by PCR amplification of a 478 bp genomic fragment from mir30c-2 (MGI:3619048) (pre-miRNA sequence, 84 bp; 187 bp and 207 bp flanking at the 5′ and 3′ sides, respectively). The primers were as follows: forward, 5′-CGCGGAT CCATTGATTAGGCATCAAG-3′ (underlined, *BamH* I); reverse, 5′-CCG GAATTCTGGGATTATAGGCACACA-3′ (underlined, *EcoR* I). Then the amplified double sequences were inserted into the *BamH* I and *EcoR* I sites in the FUGW vector after endonuclease digestion. The constructed miR-30c expression vector was also validated by sequencing.

For the assay, 400 ng of psiCHECK-2-sema3a-WT-3′UTR was transferred either alone or with 400 ng miR-30c, while 400 ng of psiCHECK-2-sema3a-MUT-3′UTR transferred with 400 ng miR-30c served as control. Two microliters of Lipofectamine 2000 (Invitrogen, Carlsbad, CA, USA) was added to HEK-293T cells plated 8–10 h earlier on 24-well plates. The activity of both firefly and *Renilla* luciferase was assessed 42 h after transfection using the Dual Luciferase Reporter kit (Promega) and a DLReady Veritas 96-well plate luminometer (Turner Biosystems). All experiments were performed in triplicate.

2.9. Statistical analysis

For microarray data, normalization was carried out using the median normalization method and clustering was done using the hierarchical method performed with average linkage and Euclidean distance metric. The GO and KEGG analysis results were specially corrected by EASE and FDR, and the significant results were defined by EASE < 0.01 and FDR < 0.01. All the other data analysis results are presented as mean ± s.d., and the differences were detected using one-way analysis of variance (ANOVA) followed by Bonferroni multiple comparisons test for qRT-PCR and dual luciferase assay results, and Dunnett T3 multiple comparisons test for immunohistochemistry results. The analyses were performed using SPSS version 20.0 (SPSS Inc. Chicago, IL) and $p < 0.05$ was considered statistically significant. The variation and correlation of sema3a expression at the mRNA and protein levels at four ages (4, 8, 14 and 19 weeks) were transformed to fold changes in comparison with 19 weeks before analyzed by Pearson's correlation coefficient (R).

3. Results

3.1. Screening of abundant microRNAs in the olfactory bulb

To analyze the microRNAs expressed in the OB of adult mice, we used the highly specific microarray after obtaining intact and pure total RNA from OBs. The hybridization results (Gene Expression Omnibus, accession no. GSE55463) showed that the signals of blank and negative controls were very low and the 5s rRNA signal used as the internal controls was strong and stable. Besides, the signals of single-nucleotide mismatched probes were clearly lower than those of the perfectly-matched probes, which indicated that the microRNA levels detected in our experiment were highly specific and accurate.

After low-intensity filtering and data normalization to the raw signals of the three microarrays, 40 sequence-unique microRNAs were found to be relatively abundant, with signals about fivefold above the median value of microarrays. These abundant microRNAs accounted for 3.69% (40 of 1084) of the total *Mus musculus* microRNAs detected by the microarray (Fig. 1A and Supplementary Table S1). Among these abundant microRNAs, 13 had already been shown to be highly expressed in the olfactory system (Hua et al., 2009; Miska et al., 2004). To validate microarray results, four microRNAs were selected for further validation by qRT-PCR (miR-200b, miR-30c, and miR-429 were enriched in axon guidance by later target prediction with the GO and KEGG enrichment results; miR-9 was chosen as comparison). The qRT-PCR results were consistent with the microarray results (Fig. 1B). Moreover, compared with the hybridization method of microarrays, qRT-PCR based on amplification was more sensitive and stable in our hands.

3.2. Target prediction and functional annotation

The bioinformatics methods are effective and direct ways for gaining insights of interested microRNAs. In this study, we selected 23 top abundant microRNAs (Supplementary Table S2) whose expressions were tenfold above the average value of the whole arrays. To enhance the reliability of target prediction, we integrated the advantages of three algorithms (TargetScan, Pita, and miRanda) by running the modified executable package files separately and then adopting the intersection results. The respective prediction results showed that microRNA–mRNA pairs were 47008 for TargetScan, 9023 for Pita, and 56449 for

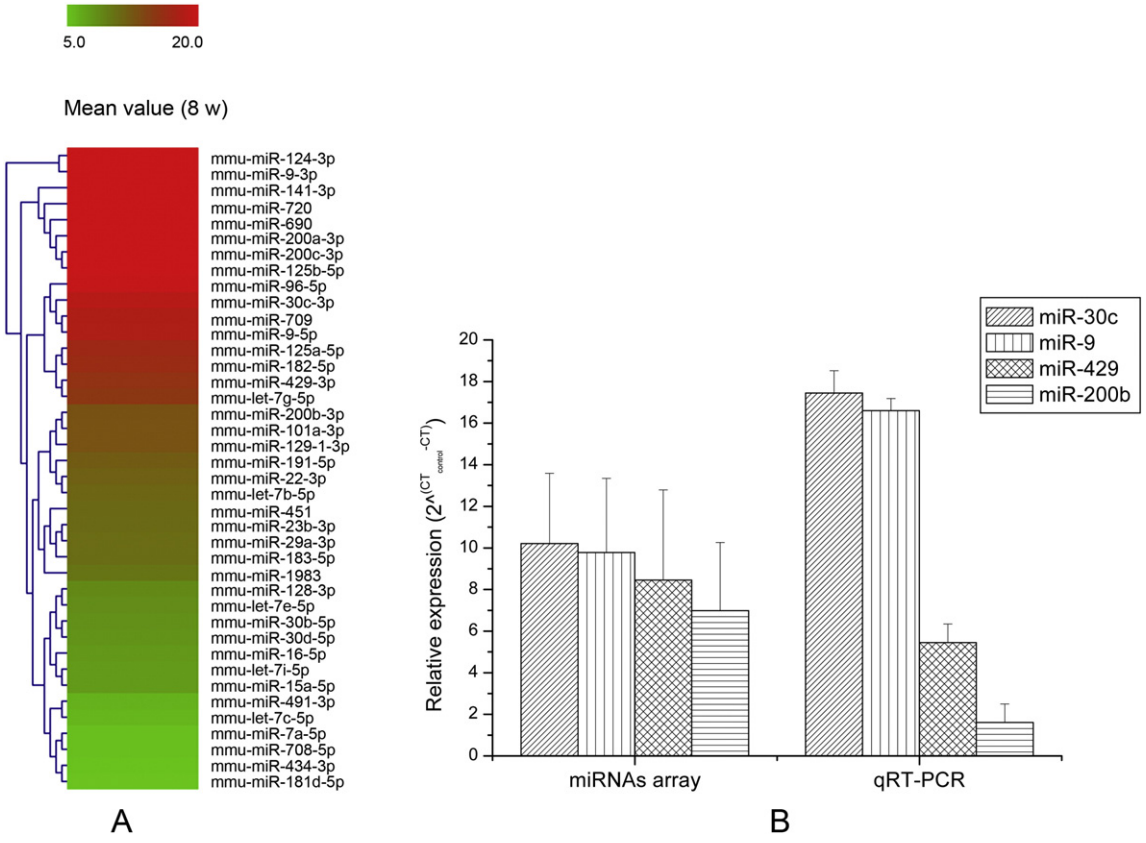

Fig. 1. microRNAs abundant in the olfactory bulb screened by LNA microarray and validated by qRT-PCR. (A) Clustering results of 40 abundant microRNAs screened from the LNA microRNA microarray (n = 3 mice). (B) Relative expression of four microRNAs detected both by miRNA array and qRT-PCR (n = 3 mice).

miRanda. The final predicted unique pairs of microRNA–mRNA were 2624 and the final unique genes were 1784 (Fig. 2) based on setting different thresholds for these algorithms to conduct a preliminary screening (For TargetScan, scores <70 were filtered out; for miRanda, results with seed = 7 were retained; and for Pita, results with $\Delta\Delta G \leq -5$ were retained). Then, to distinguish the gene functions, these 1784 target genes were carefully analyzed by GO biological process, GO cellular component, GO molecular function, and KEGG pathways, as well as Cytoscape regulatory network.

GO annotation and KEGG pathway enrichments were performed by mapping the predicted target genes from the abundant microRNAs in the OBs to the GO and KEGG databases. For the 23 abundant microRNAs, 92 GO biological processes, 13 GO cellular components, 20 GO molecular functions, and 7 KEGG pathways (all EASE < 0.01 and FDR < 0.01) were enriched in the OB. Among these enrichments, the high-enriched GO cellular components were transcription factor complex and endosome (FDR = 0.0000109 and fold enrichment = 2.42; FDR = 0.0008541 and fold enrichment = 2.16 respectively). Transcriptional reactions

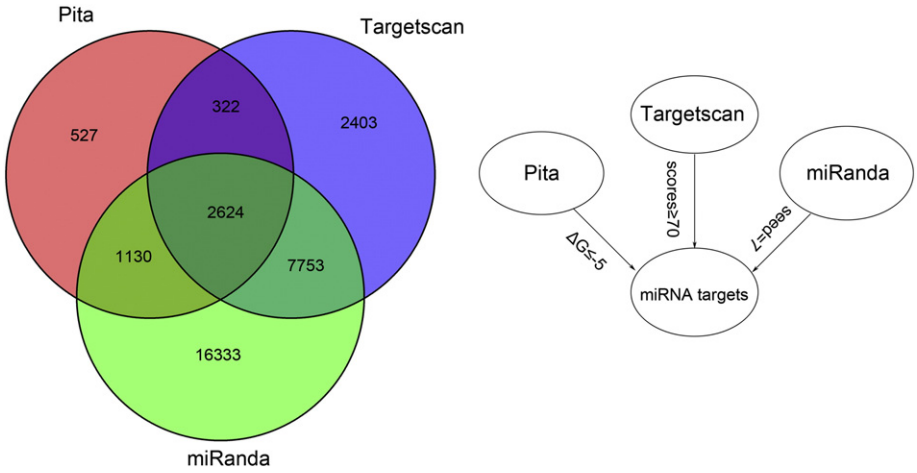

Fig. 2. Targets predicted for the 23 abundant microRNAs in the olfactory bulb by three algorithms. Left: the Venn diagram shows that there were 2624 specific microRNA–mRNA pairs from the intersection-predicted results after preliminary screening with different thresholds for the three algorithms. Right: target prediction results with $\Delta G \leq -5$ for Pita, TargetScan scores ≥ 70, and seed = 7 for miRanda were selected for Venn calculation.

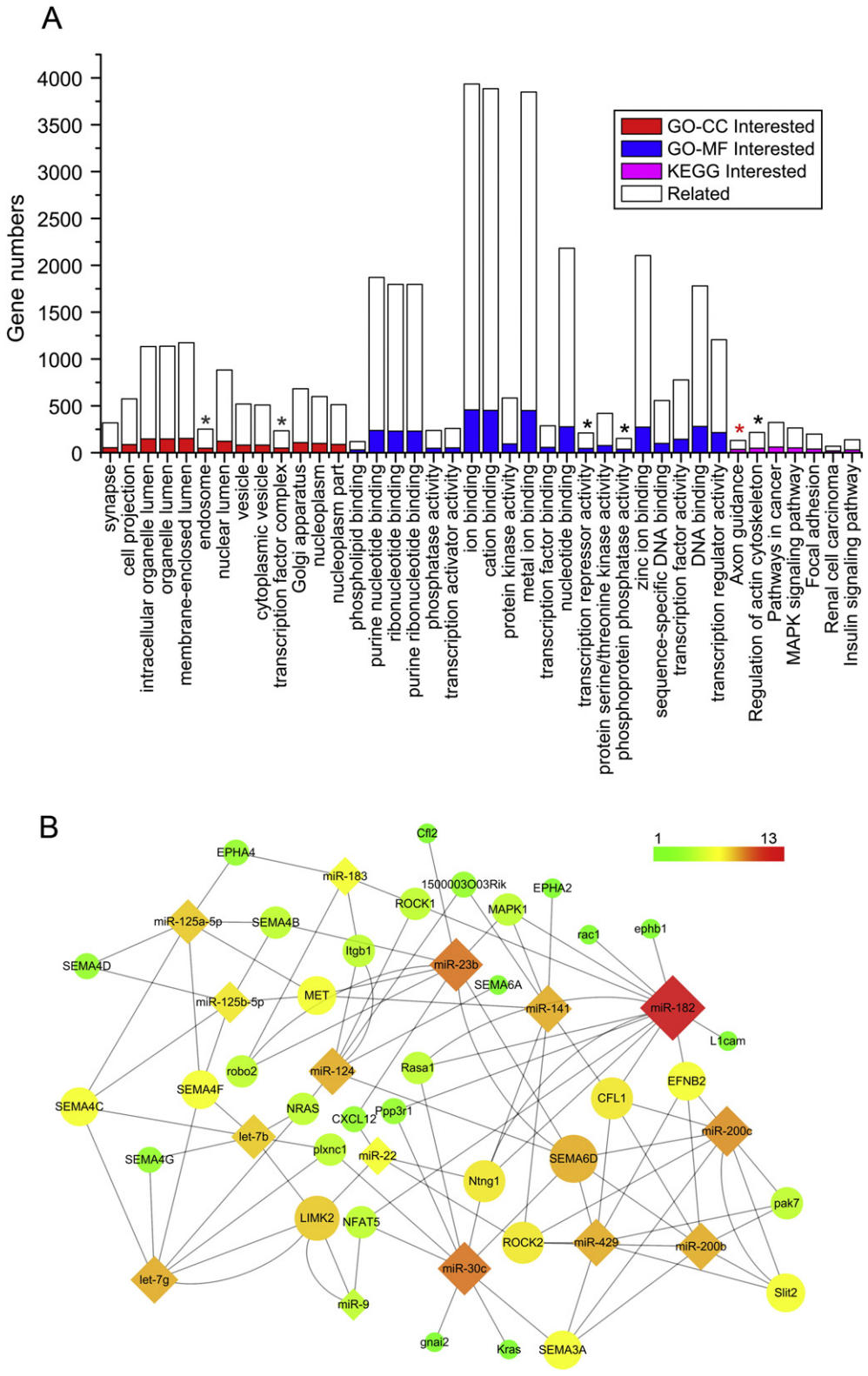

Fig. 3. GO and KEGG enrichment results for the corresponding genes of abundant microRNAs and a global view of microRNA–mRNA in the axon guidance. (A) GO and KEGG enrichments of the corresponding genes of abundant microRNAs. The categories are shown on the *x*-axis; the gene numbers for each category is shown on the *y*-axis (EASE < 0.01 and FDR < 0.01). The colored parts represent genes in the list of target genes and the white parts represent genes not in our list but associated with the corresponding terms. GO-CC, GO cellular components (red); GO-MF, GO molecular function (blue); KEGG, Kyoto Encyclopedia of Genes and Genomes (pink). The significant enrichment terms are marked with black asterisks (FDR < 0.001 and fold enrichment > 2) or red asterisks (FDR < 0.001 and fold enrichment > 3). (B) Network analysis of the enriched microRNA-target genes in axon-guidance. The size of the ellipses and diamonds indicates the degree to which microRNAs or genes contribute to the network. The minimum degree of contribution was set as one and the maximum degree of contribution was set as thirteen. The color bar in the upper right corner is a scale of contributions, contribution degree from minimum to maximum represented as a gradient color from green to red.

related functions, such as phosphoprotein phosphatase activity and transcription repressor activity (FDR = 0.0001603 and fold enrichment = 2.57; FDR = 0.0004612 and fold enrichment = 2.24, respectively), were relatively high enriched in the term of GO molecular components. In KEGG enrichments results, axon-guidance was the highest enriched pathway (FDR = 0.0000056 and fold enrichment = 3.01); the second highest-enriched pathway was regulation of actin cytoskeleton (FDR = 0.0000126 and fold enrichment = 2.44) with a threshold of FDR < 0.001 (Fig. 3A), which indicated that the main molecular and biological process in the 8-week-old OB was axon-guidance.

Furthermore, in order to clearly show the global relationship between microRNAs and their corresponding mRNAs, we transfer their relationships to microRNA–mRNA regulatory networks by Cytoscape using the internal algorithm of Prefuse Force-Directed layout. Finally, a specific connected regulatory network was extracted for the predicted target genes that were classified by pathway-specific microRNAs. We mainly focused on the highest enriched pathway, that of axon-guidance. The results showed that 15 abundant microRNAs were enriched in this pathway and 35 specific target genes of these microRNAs were included in the regulatory network (Fig. 3B). We then evaluated the topology and internal interactions of this network through network parameters. The basic parameters were analyzed with Network Analyzer plug-in. Among these acquired parameters, the most notable is the node degree distribution that reflects the model of the network. In the random model, most node degrees follow a Poisson distribution, whereas node degrees in a scale-free model have a non-uniform distribution. The node degree distribution of this network was in accordance with the power law ($y = 13.910x^{-0.846}$, $R^2 = 0.569$), indicating that the network was of scale-free and not random topology (Supplementary Fig. S1A). The other two basic network parameters are the shortest path-length, and closeness centrality, which reflect the closeness between nodes from different aspects. The shortest path-length describes the number of steps or edges along the path between two nodes, while the closeness centrality is defined as the reciprocal of the average shortest path-length. In this network, most of the path-lengths were fairly short and the closeness centrality had relatively high accordance with the power law ($y = 0.269x^{0.130}$, $R^2 = 0.470$) (Supplementary Fig. S1B and D), indicating that information in this network can be quickly transferred from a given node to other reachable nodes. Another network parameter, betweenness centrality, reflects the 'weight' of one node in the network by calculating the amount of control that this node exerts over the interactions of other nodes, the betweenness centrality of this network fitted a power law ($y = 0.001x^{2.266}$, $R^2 = 0.416$), indicating that several nodes made unequal contributions to the network (Supplementary Fig. S1C) (Doncheva et al., 2012). miR-182, miR-23, and miR-30c of this network were such nodes, and they have relatively more relationships with others in axon guidance pathway, as their icons were relatively larger and colors tended to the red side of the gradient color bar (Fig. 3B). As the role of sema3a in axon-guidance has been well characterized

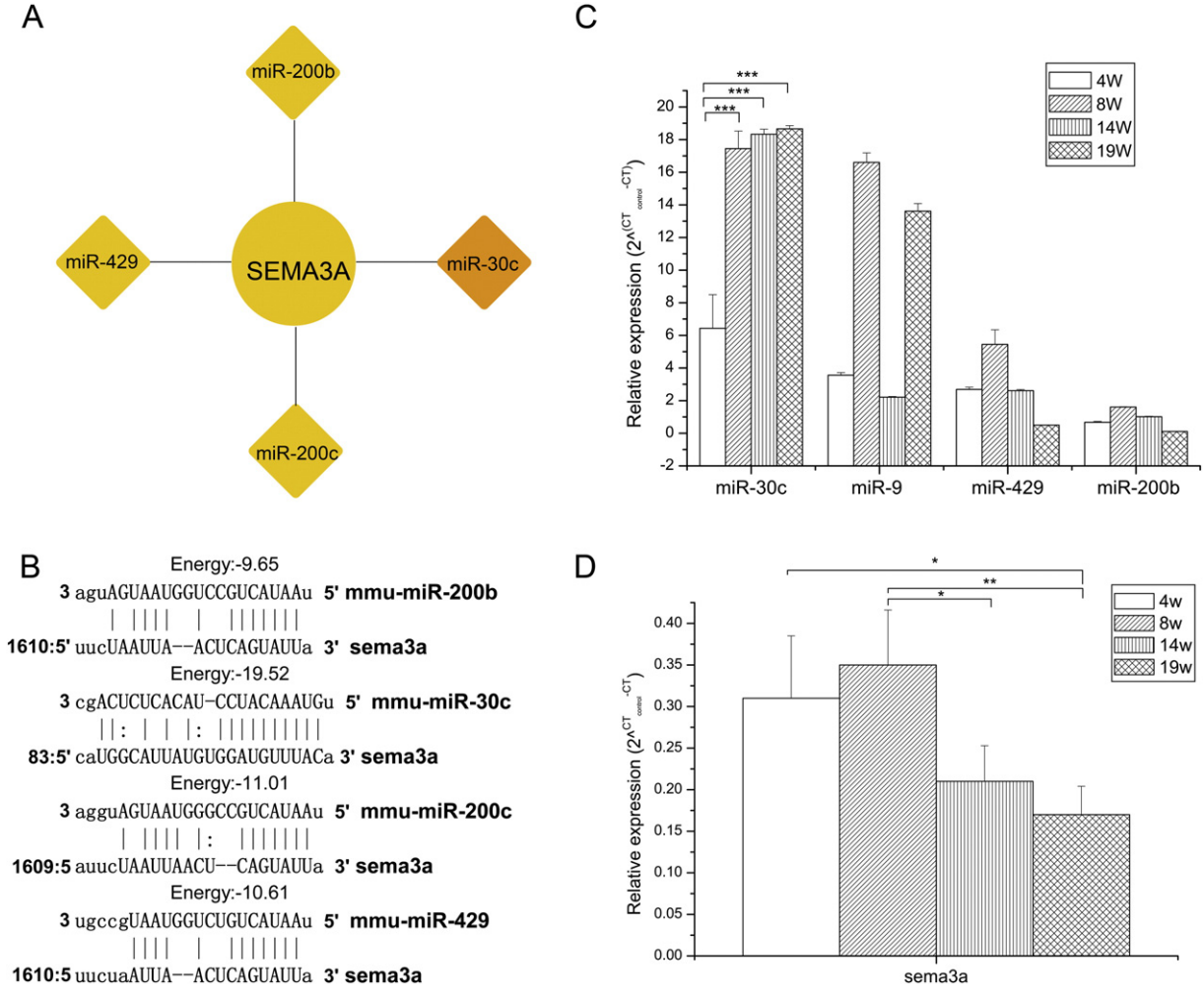

Fig. 4. Validation of candidate regulators of sema3a. (A) Four candidate regulators of sema3a adopted from the predicted results of three algorithms (TargetScan, Pita, miRanda). (B) The binding sites of four microRNAs to the 3′ UTR of sema3a and their respective binding energy. (C) miR-30c had a relatively better corresponding expression pattern to sema3a. The expression patterns of four microRNAs and sema3a were traced using mice at different ages (4, 8, 14, and 19 weeks) *via* qRT-PCR (n = 3 mice per age group). All samples passed the Kolmogorov–Smirnov normality test. ANOVA followed by Bonferroni post-test. Values are shown as the mean ± s.d. (*$p < 0.05$, **$p < 0.01$, ***$p < 0.001$).

in nervous system and it is crucial in the development of OB, to find the microRNA regulator of sema3a, we chose sema3a and its predicted regulatory microRNAs for validating the target–regulator relationships.

3.3. Validation of a potential regulator of sema3a

To better analyze the target–regulator relationship between sema3a and its corresponding microRNAs, we extracted sema3a and its candidate microRNAs miR-30c, miR-200b, miR-200c, and miR-429 from the microRNA–mRNA networks (Fig. 4A) and then explored the binding sites of these microRNAs with sema3a *via* miRanda. The results showed that miR-30c had a high binding score for sema3a than the other three (miR-30c, $\Delta\Delta G < -19.52$; miR-200b, $\Delta\Delta G < -9.65$; miR-200c, $\Delta\Delta G < -11.01$; miR-429, $\Delta\Delta G < -10.61$). Moreover, the results showed that miR-200b, miR-200c, and miR-429 have nearly identical binding sites on the 3′ UTR region of sema3a, while miR-30c has different binding sites. This suggested that miR-200b, miR-200c, and miR-429 probably have similar functions by synergistically binding the same region of mRNA, while miR-30c may have a distinct function from the other three (Fig. 4B).

The primers (Supplementary Table S3) specific to these four microRNAs (miR-30c, miR-200b, miR-9, and miR-429) were used for qRT-PCR analysis (as miR-200b and miR-200c belong to the same family and share the same seed sequence, we selected miR-200b for qRT-PCR analysis), and simultaneously, miR-9, an abundant microRNA in brain, was added as comparison to estimate the expression of microRNAs in OBs at different ages. The expression pattern of the candidate microRNAs and sema3a were traced with age. As a result, the expression of miR-30c was higher than miR-9 in all the ages traced, while that of miR-200b and miR-429 was lower than miR-9. Besides, there was a good corresponding inverse expression pattern between miR-30c and sema3a from 8 weeks to 19 weeks. During this time span, the

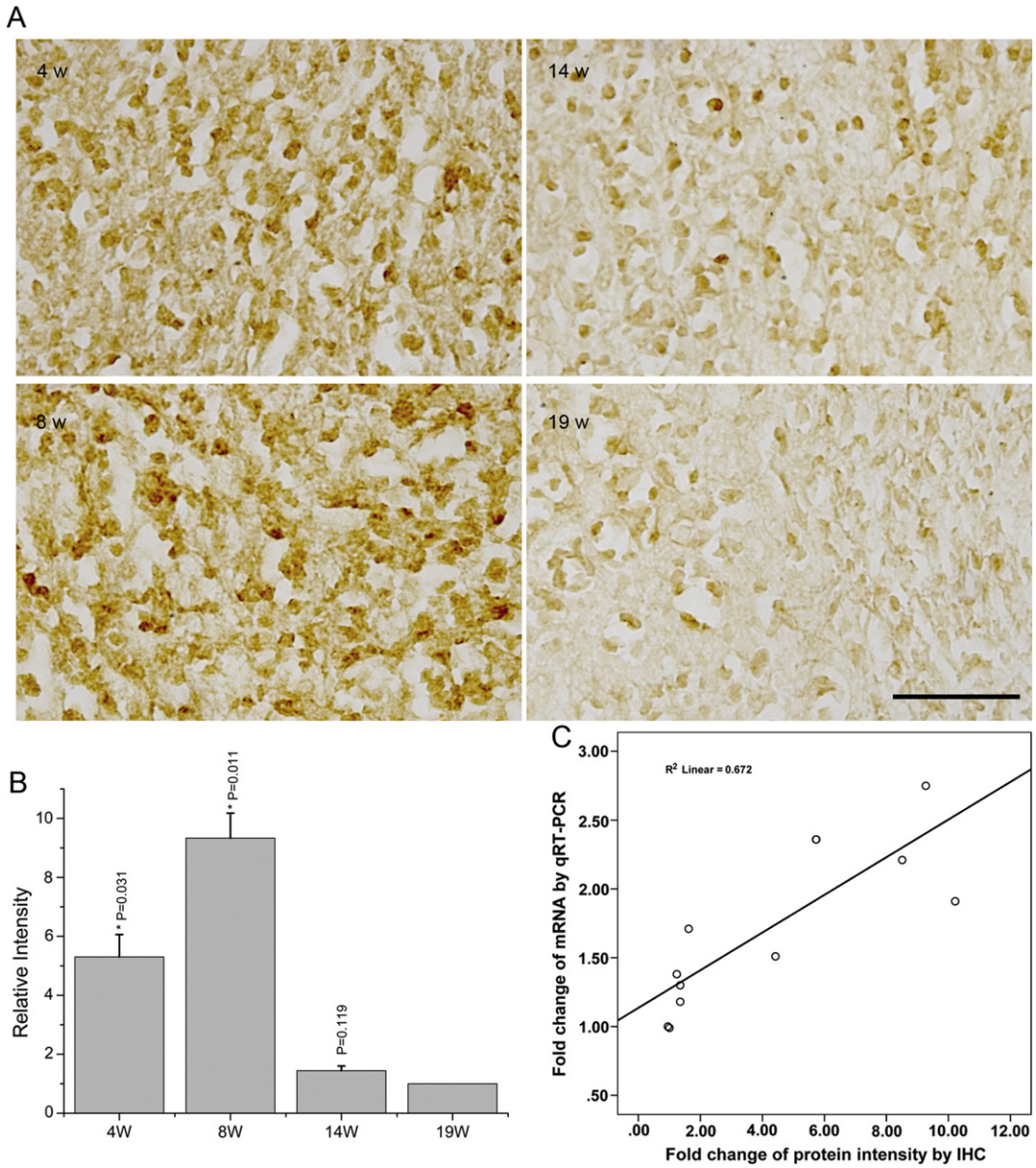

Fig. 5. Expression of Sema3a at different ages. (A) Expression of sema3a in the granule-cell layer (at 4, 8, 14, and 19 weeks; n = 3 mice per age group). Scale bar, 50 μm. (B) Quantification of sema3a expression in the granule-cell layer by calculating three biological regions of the layer at each age with IPP (version 6.0).*$p < 0.05$, determined by one-way ANOVA. Data are shown as the mean ± s.d. and values were normalized to the intensity of sema3a in the 19 weeks. (C) Pearson correlation scatter-plot of protein and nucleotide levels of sema3a. The *x*-axis is the fold-change of protein intensity of sema3a detected by immunohistochemistry (IHC) and the *y*-axis is the fold-change of mRNA of sema3a detected by qRT-PCR (n = 12, $p = 0.001$) (correlation significant at the 0.01 level; Pearson's correlation coefficient using SPSS version 20.0).

expression of miR-30c continuously increased (Fig. 4C) while sema3a continuously declined from age of 8 weeks (Fig. 4D). Also, the expression pattern of sema3a was further validated in protein level by immunohistochemistry results, which were highly consistent with the qRT-PCR results, with a correlation coefficient of 0.820 (Fig. 5C). All of the results above indicated that miR-30c is the most potential regulator of sema3a.

3.4. Test of the regulatory relationship between miR-30c and sema3a

To further validate the target–regulator relationship between sema3a and miR-30c, the expression and location of sema3a at different ages were detected. In addition to the olfactory neuron layer and periglomerular layer, the reported main distribution of sema3a, sema3a had relatively abundant expression in the granule-cell layer (Fig. 5A). Moreover, the expression of sema3a first increased and then declined with peak at 8 weeks (Fig. 5B). The pattern of sema3a expression detected by immunochemistry was consistent with the quantification results of sema3a by qRT-PCR, with a correlation coefficient of 0.820 (Pearson correlation, two-tailed, n = 12, $p = 0.001$) (Fig. 5C).

To finally determine the target–regulator relationship between sema3a and miR-30c, we performed the dual luciferase assay by constructing a psiCHECK-2-sema3a-WT-3′ UTR vector, psiCHECK-2-sema3a-MUT-3′ UTR vector, and miR-30c expression vector. The results showed that when the psiCHECK-2-sema3a-WT-3′ UTR was co-transfected with the miR-30c expression vector, sema3a expression was markedly reduced (by 41%–105%) comparing with psiCHECK-2-sema3a-WT-3′ UTR transfected alone ($F_{2,6} = 28.61$, $p = 0.0009$). However, when the psiCHECK-2-sema3a-MUT-3′ UTR was transfected together with the miR-30c, the expression of sema3a was similar to that of psiCHECK-2-sema3a-WT-3′ UTR transfected alone ($F_{2,6} = 28.61$, $p = 0.1670$) (Fig. 6), indicating that the suppressive effect of miR-30c on sema3a expression can be rescued by mutation in the binding

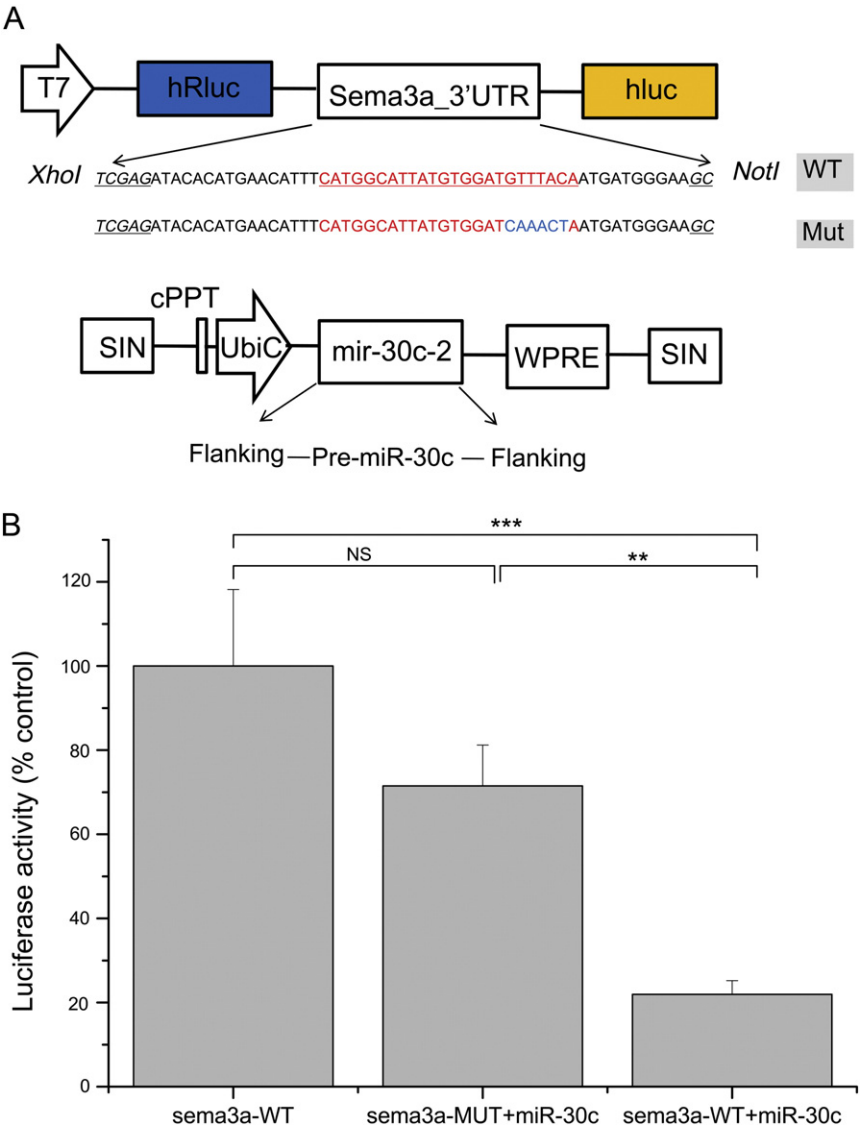

Fig. 6. Dual luciferase activity measurements. (A) Dual luciferase assay vector construction. sema3a-3′ UTR sequence (GI: 340523098, NM_009152) was inserted into the psiCHECK-2 vector by multiple clone sites of *Xho*I and *Not* I (italic). Nucleotides predicted to bind with miR-30c are in red and mutant sites in the mutant are in blue. Pre-miR-30c (MI0000548) with 5′ and 3′ flanking sequences was cloned into FUGW to construct the expression vector of miR-30c (WT, wild type; Mut, mutant). (B) Quantification of dual luciferase activity. The miR-30c expression vector was co-transfected with psiCHECK-2-sema3a-WT-3′UTR or psiCHECK-2-sema3a-MUT-3′UTR in HEK-293T (human embryonic kidney) cells (n = 3 wells), values were normalized to luciferase intensity of wells that only transfected with sema3a-WT vector. All samples passed the Kolmogorov–Smirnov normality test. ANOVA followed by Bonferroni post-test. Values are shown as the mean ± s.d. (NS, not significant,$^{**}p < 0.01$, $^{***}p < 0.001$).

site between sema3a and miR-30c. So our data suggested that miR-30c can suppress the expression of sema3a by the specific binding sites on sema3a.

4. Discussion

4.1. Axon guidance is the main molecular and biological process ongoing in the steady-state olfactory bulb of the adult mouse

The OB is a tightly-organized architecture and its ability to process sensory information depends on the ordered structure and synaptic connectivity patterns of the underlying neuronal circuits. The general architecture of the circuits is laid down from early in the embryonic development to the first several days after birth (Schwarting et al., 2000). But olfactory neurons and interneurons are continuously replaced by the stem-like cells coming from the basal and subventricular zones, respectively (Lledo et al., 2006). Genetic *in vivo* imaging revealed that the turnover of neurons in the periglomerular layer is ~3% per month, so about 30% of this population is replaced after nine months (Mizrahi et al., 2006; Ninkovic et al., 2007). Besides, when the path along which OB neuron precursors migrate is blocked, the size of the OB is reduced ~40% and odor discrimination is impaired (Gheusi et al., 2000). So the adult newborn neurons probably migrate to their fitted places under the guidance of axon-guidance cues, which expected to continue to refine the stereotypical structure and function of the adult OB.

The results of our bioinformatics analysis showed that corresponding genes of the abundant microRNAs mainly constitute transcription factor complexes engaging in phosphatase reactions, transcription or repressor processes, which are closely associated with proteins synthesis. Also the KEGG enrichment results showed that axon-guidance was the most enriched pathway in the OB. These results are consistent with the report that both growing and mature axons possess a complex and dynamic transcriptome and this local mRNA translation can mediate directional responses to guidance signals (Martin, 2004). Thus, axon guidance cues probably play roles in the processes of assembly, maintenance, and repair of the OB through local mRNA translation. As in the nervous system, Netrin-1, a member of a family of secreted proteins, has been discovered to participate in the maintenance and plasticity of connections in the adult brain (Hakanen et al., 2011). Similarly, another axon-guidance family, the ephrins, has been reported to play important roles in neuron–target interactions and synaptic connectivity, in the mature peripheral vestibular system (Matsunaga et al., 2000). Since a series of events occurs exclusively in the adult OB, such as the dynamic turnover of interneurons and sexual differentiation (Ninkovic et al., 2007; Tsim et al., 2004), it is possible that axon guidance is the main molecular and biological process to enable the adult OB to complete these specific tasks.

4.2. MiR-30c is the most likely regulator of sema3a

MicroRNAs are endogenously-expressed noncoding RNAs that regulate mRNA expression. Many microRNAs are specifically expressed in the nervous system, where they modulate neurite outgrowth, dendritogenesis, and spine formation by locally regulating protein transcription in the axosomal and synaptodendritic compartments. Due to their regulation of the transcription of specific proteins, microRNAs emerged as determinants of neuronal survival, regeneration, and differentiation (Li and Jin, 2010; Olde Loohuis et al., 2012). As the adult OB continuously accommodates newborn neurons from the subventricular zone, the processes of neuronal survival, apoptosis, and specific synapse formation are ongoing in the adult OB, so microRNAs are potentially involved in the maintenance of the circuits structure by regulating sema3a, an active axon-guidance cue in the OB (Baudet et al., 2013).

To explore microRNAs that function in maintaining the adult OB, we used microRNA expression microarrays, and the profile showed that

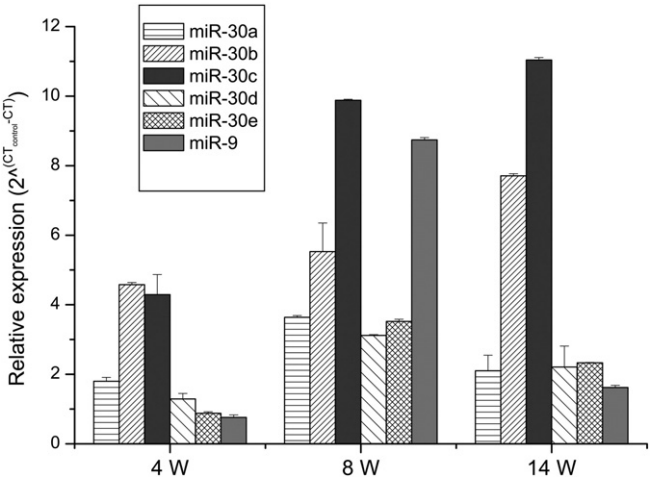

Fig. 7. Expression levels of miR-30 family members with age by qRT-PCR (miR-9 was added for comparison, n = 3–5 mice per age group).

miR-30c was abundant in the adult OB. Also, it was the most abundant member of the miR-30 family from 4 to 14 weeks, according to qRT-PCR analysis with stem-loop specific primers (Fig. 7). Recently, it has been reported that miR-30c is abundant in many tissues and its expression level is higher than that of other family members, such as miR-30e (Soh et al., 2013). These results suggest that miR-30c probably take a more important role in the adult OB, given its higher expression than the other family members. Despite the fact that they share same seed sequence, members of the miR-30 family have distinct functions. MiR-30a plays a role in *Xenopus* kidney development (Agrawal et al., 2009) and miR-30e regulates apoptosis in breast tumor cells (Yu et al., 2010). The intersection-predicted results of three bioinformatics algorithms suggested that miR-30c as well as miR-200b, miR-200c, and miR-429 are the candidate regulators of sema3a.

To identify the potential regulators of sema3a, we traced the expression patterns of the four candidate microRNAs and sema3a from 4 to 19 weeks. The results showed that only miR-30c had the corresponding inverse expression pattern with sema3a. Moreover, the double luciferase assay demonstrated that miR-30c suppressed the sema3a expression mainly by binding to its 3′ UTR *via* the seed region (Fig. 6).

In conclusion, we screened 40 abundant microRNAs in the adult OB. About 65% (15/23) of the top abundant microRNAs are enriched in axon guidance and miR-30c was identified to be a regulator of sema3a, indicating that miR-30c takes part in axon guidance *via* modulating the expression of sema3a. All our results will enable further in-depth testing of microRNA roles in development and maintenance of neuronal circuits, as well as turnover of interneurons in OB.

Supplementary data to this article can be found online at http://dx.doi.org/10.1016/j.gene.2014.06.063.

Disclosure of conflict of interest

None.

Acknowledgments

We thank Prof. Iain Charles Bruce, Department of Neurobiology, Zhejiang University School of Medicine, for corrections to the English text and Prof. Jingwei Zhao, Department of Neurobiology, Zhejiang University School of Medicine, for corrections and suggestions to the article. This work was partly supported by the National Natural Science Foundation of China (81371404).

References

Agrawal, R., Tran, U., Wessely, O., 2009. The miR-30 miRNA family regulates *Xenopus* pronephros development and targets the transcription factor Xlim1/Lhx1. Development 136, 3927–3936.

Baudet, M.L., Bellon, A., Holt, C.E., 2013. Role of microRNAs in semaphorin function and neural circuit formation. Semin. Cell Dev. Biol. 24, 146–155.

Causeret, F., 2006. Differential role of slits in dorsal versus ventral retinal axon guidance. J. Neurosci. 26, 9839–9840.

Chen, H., He, Z., Tessier-Lavigne, M., 1998. Axon guidance mechanisms: semaphorins as simultaneous repellents and anti-repellents. Nat. Neurosci. 1, 436–439.

Chen, C., Ridzon, D.A., Broomer, A.J., Zhou, Z., Lee, D.H., Nguyen, J.T., Barbisin, M., Xu, N.L., Mahuvakar, V.R., Andersen, M.R., Lao, K.Q., Livak, K.J., Guegler, K.J., 2005. Real-time quantification of microRNAs by stem-loop RT-PCR. Nucleic Acids Res. 33, e179.

Cheng, L.C., Pastrana, E., Tavazoie, M., Doetsch, F., 2009. miR-124 regulates adult neurogenesis in the subventricular zone stem cell niche. Nat. Neurosci. 12, 399–408.

Choi, P.S., Zakhary, L., Choi, W.Y., Caron, S., Alvarez-Saavedra, E., Miska, E.A., McManus, M., Harfe, B., Giraldez, A.J., Horvitz, H.R., Schier, A.F., Dulac, C., 2008. Members of the miRNA-200 family regulate olfactory neurogenesis. Neuron 57, 41–55.

Cohen, R.I., Rottkamp, D.M., Maric, D., Barker, J.L., Hudson, L.D., 2003. A role for semaphorins and neuropilins in oligodendrocyte guidance. J. Neurochem. 85, 1262–1278.

de Chevigny, A., Core, N., Follert, P., Gaudin, M., Barbry, P., Beclin, C., Cremer, H., 2012. miR-7a regulation of Pax6 controls spatial origin of forebrain dopaminergic neurons. Nat. Neurosci. 15, 1120–1126.

Doncheva, N.T., Assenov, Y., Domingues, F.S., Albrecht, M., 2012. Topological analysis and interactive visualization of biological networks and protein structures. Nat. Protoc. 7, 670–685.

Finger, J.H., Bronson, R.T., Harris, B., Johnson, K., Przyborski, S.A., Ackerman, S.L., 2002. The netrin 1 receptors Unc5h3 and Dcc are necessary at multiple choice points for the guidance of corticospinal tract axons. J. Neurosci. 22, 10346–10356.

Gheusi, G., Cremer, H., McLean, H., Chazal, G., Vincent, J.D., Lledo, P.M., 2000. Importance of newly generated neurons in the adult olfactory bulb for odor discrimination. Proc. Natl. Acad. Sci. U. S. A. 97, 1823–1828.

Hakanen, J., Duprat, S., Salminen, M., 2011. Netrin1 is required for neural and glial precursor migrations into the olfactory bulb. Dev. Biol. 355, 101–114.

Han, Z.B., Zhong, L., Teng, M.J., Fan, J.W., Tang, H.M., Wu, J.Y., Chen, H.Y., Wang, Z.W., Qiu, G.Q., Peng, Z.H., 2012. Identification of recurrence-related microRNAs in hepatocellular carcinoma following liver transplantation. Mol. Oncol. 6, 445–457.

Hojati, Z., Orangi, E., 2012. HER-2/neu gene amplification assessment in breast cancer patients in Isfahan province by real time PCR, differential PCR and immunohistochemistry. Gene 497, 237–242.

Hosack, D.A., Dennis Jr., G., Sherman, B.T., Lane, H.C., Lempicki, R.A., 2003. Identifying biological themes within lists of genes with EASE. Genome Biol. 4, R70.

Hua, Y.J., Tang, Z.Y., Tu, K., Zhu, L., Li, Y.X., Xie, L., Xiao, H.S., 2009. Identification and target prediction of miRNAs specifically expressed in rat neural tissue. BMC Genomics 10, 214.

Imai, T., Yamazaki, T., Kobayakawa, R., Kobayakawa, K., Abe, T., Suzuki, M., Sakano, H., 2009. Pre-target axon sorting establishes the neural map topography. Science 325, 585–590.

Lakhina, V., Marcaccio, C.L., Shao, X., Lush, M.E., Jain, R.A., Fujimoto, E., Bonkowsky, J.L., Granato, M., Raper, J.A., 2012. Netrin/DCC signaling guides olfactory sensory axons to their correct location in the olfactory bulb. J. Neurosci. 32, 4440–4456.

Li, X., Jin, P., 2010. Roles of small regulatory RNAs in determining neuronal identity. Nat. Rev. Neurosci. 11, 329–338.

Lledo, P.M., Alonso, M., Grubb, M.S., 2006. Adult neurogenesis and functional plasticity in neuronal circuits. Nat. Rev. Neurosci. 7, 179–193.

Luo, Y., Raible, D., Raper, J.A., 1993. Collapsin: a protein in brain that induces the collapse and paralysis of neuronal growth cones. Cell 75, 217–227.

Martin, K.C., 2004. Local protein synthesis during axon guidance and synaptic plasticity. Curr. Opin. Neurobiol. 14, 305–310.

Matsunaga, T., Greene, M.I., Davis, J.G., 2000. Distinct expression patterns of Eph receptors and ephrins relate to the structural organization of the adult rat peripheral vestibular system. Eur. J. Neurosci. 12, 1599–1616.

Miska, E.A., Alvarez-Saavedra, E., Townsend, M., Yoshii, A., Sestan, N., Rakic, P., Constantine-Paton, M., Horvitz, H.R., 2004. Microarray analysis of microRNA expression in the developing mammalian brain. Genome Biol. 5, R68.

Mizrahi, A., Lu, J., Irving, R., Feng, G., Katz, L.C., 2006. In vivo imaging of juxtaglomerular neuron turnover in the mouse olfactory bulb. Proc. Natl. Acad. Sci. U. S. A. 103, 1912–1917.

Ninkovic, J., Mori, T., Gotz, M., 2007. Distinct modes of neuron addition in adult mouse neurogenesis. J. Neurosci. 27, 10906–10911.

Olde Loohuis, N.F., Kos, A., Martens, G.J., Van Bokhoven, H., Nadif Kasri, N., Aschrafi, A., 2012. MicroRNA networks direct neuronal development and plasticity. Cell. Mol. Life Sci. 69, 89–102.

Polleux, F., Morrow, T., Ghosh, A., 2000. Semaphorin 3A is a chemoattractant for cortical apical dendrites. Nature 404, 567–573.

Puschmann, T.B., Turnley, A.M., 2010. Eph receptor tyrosine kinases regulate astrocyte cytoskeletal rearrangement and focal adhesion formation. J. Neurochem. 113, 881–894.

Schwarting, G.A., Kostek, C., Ahmad, N., Dibble, C., Pays, L., Puschel, A.W., 2000. Semaphorin 3A is required for guidance of olfactory axons in mice. J. Neurosci. 20, 7691–7697.

Shelly, M., Cancedda, L., Lim, B.K., Popescu, A.T., Cheng, P.L., Gao, H., Poo, M.M., 2011. Semaphorin3A regulates neuronal polarization by suppressing axon formation and promoting dendrite growth. Neuron 71, 433–446.

Soh, J., Iqbal, J., Queiroz, J., Fernandez-Hernando, C., Hussain, M.M., 2013. MicroRNA-30c reduces hyperlipidemia and atherosclerosis in mice by decreasing lipid synthesis and lipoprotein secretion. Nat. Med. 19, 892–900.

Sweeney, L.B., Chou, Y.H., Wu, Z., Joo, W., Komiyama, T., Potter, C.J., Kolodkin, A.L., Garcia, K.C., Luo, L., 2011. Secreted semaphorins from degenerating larval ORN axons direct adult projection neuron dendrite targeting. Neuron 72, 734–747.

Taniguchi, M., Yuasa, S., Fujisawa, H., Naruse, I., Saga, S., Mishina, M., Yagi, T., 1997. Disruption of semaphorin III/D gene causes severe abnormality in peripheral nerve projection. Neuron 19, 519–530.

Taniguchi, M., Nagao, H., Takahashi, Y.K., Yamaguchi, M., Mitsui, S., Yagi, T., Mori, K., Shimizu, T., 2003. Distorted odor maps in the olfactory bulb of semaphorin 3A-deficient mice. J. Neurosci. 23, 1390–1397.

Tessier-Lavigne, M., Goodman, C.S., 1996. The molecular biology of axon guidance. Science 274, 1123–1133.

Tsim, T.Y., Wong, E.Y., Leung, M.S., Wong, C.C., 2004. Expression of axon guidance molecules and their related genes during development and sexual differentiation of the olfactory bulb in rats. Neuroscience 123, 951–965.

Wang, B., Dong, M., Chen, W., Liu, X., Feng, R., Xu, T., 2012. Microarray identification of conserved microRNAs in *Pinellia pedatisecta*. Gene 498, 36–40.

Yu, F., Deng, H., Yao, H., Liu, Q., Su, F., Song, E., 2010. Mir-30 reduction maintains self-renewal and inhibits apoptosis in breast tumor-initiating cells. Oncogene 29, 4194–4204.